Single slepton production in association with a single top quark at the Fermilab Tevatron and CERN LHC

M. A. Bernhardt,[*] H. K. Dreiner,[+] and S. Grab[‡]
Physikalisches Institut, University of Bonn, Bonn, Germany

P. Richardson[§]
IPPP, University of Durham, Durham, United Kingdom and Theoretical Physics Group, CERN, Geneva, Switzerland
(Received 12 March 2008; published 24 July 2008)

We calculate the total cross section for single charged slepton production in association with a top quark at hadron colliders in the baryon-triality (B_3) supersymmetric model. We compute event rates for the Fermilab Tevatron and CERN LHC. We study the signatures for different supersymmetric scenarios including neutralino and stau lightest supersymmetric particles. We perform a detailed analysis with basic cuts for the B_3 operator λ'_{231} using Monte Carlo simulations to show that the signal can be distinguished from the background at the LHC. In particular, we employ the resulting lepton charge asymmetry.

DOI: 10.1103/PhysRevD.78.015016 PACS numbers: 12.60.Jv, 13.85.Lg, 14.65.Ha, 14.80.Ly

I. INTRODUCTION

Supersymmetry (SUSY) [1] is a widely considered extension of the standard model (SM) of particle physics [2]. If it exists, it is necessarily broken, with a mass scale of order of the TeV energy scale [3]. This energy region is probed at both the Fermilab Tevatron and CERN LHC; the search for SUSY is therefore of paramount interest [4,5]. It is the purpose of this paper to consider a specific supersymmetric production mechanism and investigate its viability at the Tevatron and LHC.

The general renormalizable superpotential with minimal particle content [6] includes the following lepton or baryon number violating interactions,

$$W_{\not P_6} = \epsilon_{ab}[\tfrac{1}{2}\lambda_{ijk}L_i^a L_j^b \bar{E}_k + \lambda'_{ijk}L_i^a Q_j^{bx}\bar{D}_{kx}] + \epsilon_{ab}\kappa^i L_i^a H_2^b + \tfrac{1}{2}\epsilon_{xyz}\lambda''_{ijk}\bar{U}_i^x \bar{D}_j^y \bar{D}_k^z, \quad (1.1)$$

where we have employed the standard notation of Ref. [7] for the superfields, couplings, and indices. If all terms are simultaneously present, they lead to rapid proton decay [8]. Therefore SUSY must be augmented by an additional symmetry. The discrete anomaly-free gauge symmetries R-parity [9] and proton hexality, P_6 [10], forbid all of the above terms. However, R-parity does not forbid the dangerous dimension-five proton decay operators [6].

An equally well-motivated solution to the proton decay problem is baryon triality, B_3, a discrete anomaly-free $\boldsymbol{Z}_3$ symmetry, which prohibits the $\bar{U}\bar{D}\bar{D}$ operator in Eq. (1.1) [11–13]. This solution has an additional feature; it naturally leads to small neutrino masses [14–20], as experimentally observed [21]. Furthermore, B_3 supersymmetric models, which include also a candidate for dark matter, have been, for example, constructed in Refs. [22].

The baryon-triality collider phenomenology has three main distinguishing features, compared to the P_6 case [7,23]:

(1) The lightest supersymmetric particle (LSP) is not stable and can decay in the detector. It also need not be the lightest neutralino.
(2) SUSY particles are also produced singly, possibly on resonance.
(3) Lepton flavor and number are violated.

These lead to dramatically different signatures at hadron colliders [23–26] compared to the more widely studied P_6 case.

In the following, we focus solely on the signatures due to a nonvanishing $L_i Q_j \bar{D}_k$ operator. At hadron colliders this allows resonant single slepton and sneutrino production via incoming quarks,

$$\bar{u}_j + d_k \xrightarrow{\lambda'_{ijk}} \tilde{\ell}_i^-, \quad (1.2)$$

$$\bar{d}_j + d_k \xrightarrow{\lambda'_{ijk}} \tilde{\nu}_i. \quad (1.3)$$

Here, u_j and d_k denote up- and down-type quarks of generations j and k, respectively; a bar denotes an antiquark; $\tilde{\ell}_i^-$ and $\tilde{\nu}_i$ denote negatively charged sleptons and sneutrinos of generation i, respectively.

The tree-level processes, Eqs. (1.2) and (1.3), were first considered in Refs. [27,28]. Like-sign dilepton events or three lepton final states were considered in Refs. [29–31]. These papers assume a neutralino LSP, which can decay leptonically via λ'_{ijk}, e.g. $\tilde{\chi}_1^0 \to \ell_i^+ \bar{u}_j d_k$. The case of a gravitino LSP was considered in Ref. [32]. The process

[*]markus@th.physik.uni-bonn.de
[+]dreiner@th.physik.uni-bonn.de
[‡]sgrab@th.physik.uni-bonn.de
[§]Peter.Richardson@durham.ac.uk

TABLE I. Upper 2σ bounds on λ'_{i3k}. The strong bounds on λ'_{i33} stem from neutrino masses m_ν, assuming $m_\nu < 1$ eV and left-right mixing in the sbottom sector. The limits depend on the squark masses; $m_{\tilde{q}_{L(R)}}$ is the mass of the left- (right-) handed squark $\tilde{q}_{L(R)}$.

λ'_{131}	$0.019 \times (m_{\tilde{t}_L}/100\ \text{GeV})$	λ'_{132}	$0.28 \times (m_{\tilde{t}_L}/100\ \text{GeV})$
λ'_{231}	$0.18 \times (m_{\tilde{b}_L}/100\ \text{GeV})$	λ'_{232}	$0.45\,(m_{\tilde{s}_R} = 100\ \text{GeV})$
λ'_{331}	$0.45\,(m_{\tilde{q}} = 100\ \text{GeV})$	λ'_{332}	$0.45\,(m_{\tilde{q}} = 100\ \text{GeV})$
λ'_{i33}	$\mathcal{O}(10^{-4})$		

has also been studied by the D0 Collaboration at the Tevatron [33,34], for the operator $L_2 Q_1 \bar{D}_1$ and a neutralino LSP, setting limits on the relevant masses and couplings. In Refs. [35–38] the next-to-leading order (NLO) corrections in QCD were considered, and in Ref. [37] the SUSY-QCD corrections were taken into account. Gluon fusion contributions were included in Ref. [38].

The case $j = 3$ in Eq. (1.2) is special, as there are no top quarks in the incoming proton. Instead, one must consider the production of a single slepton in association with a SM particle. Several mechanisms for associated single supersymmetry production, e.g. $d_j \bar{d}_k \to \tilde{\chi}_1^+ \ell_i^-$, have been studied in the literature; see, for example, Refs. [31,39–42]. In the following, we investigate in detail the case of the operator $L_i Q_3 \bar{D}_k$. Here, single charged slepton production is only possible in association with a top quark. Before studying the phenomenological details, we first recall the strongest experimental bounds on the couplings λ'_{i3k} at the 2σ level. They are shown in Table I [7,23,43–45]. We neglect bounds which assume a specific (standard model) quark mixing between the three generations [46] or bounds using the renormalization group running of λ'_{i3k} [18,45,47].

At leading order there are two production mechanisms for slepton production in association with a top quark. The first mechanism includes the Compton-like processes

$$g + d_k \to \tilde{\ell}_i^- + t, \tag{1.4a}$$

$$g + \bar{d}_k \to \tilde{\ell}_i^+ + \bar{t}. \tag{1.4b}$$

The relevant leading-order diagrams are given in Fig. 1. Here, g denotes an incoming gluon in the proton and t a final-state top quark.

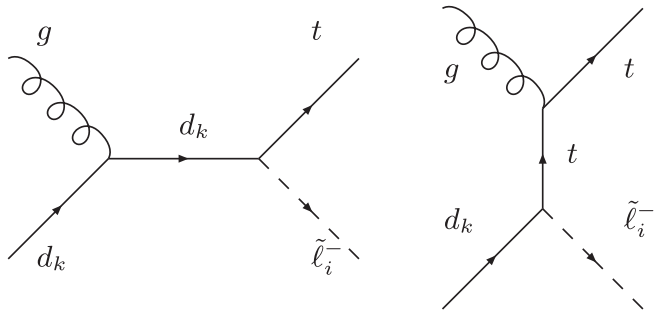

FIG. 1. Feynman diagrams contributing to the partonic process $g + d_k \to t + \tilde{\ell}_i^-$.

The second slepton production mechanism is $t\bar{t}$ pair production followed by the t or $\bar{t}$ decaying into $\tilde{\ell}_i^+$ or $\tilde{\ell}_i^-$, respectively. The main production mechanisms for $t\bar{t}$ production, at $O(\alpha_s^2)$, are

$$\left.\begin{aligned} q + \bar{q} &\to t + \bar{t} \\ g + g &\to t + \bar{t} \end{aligned}\right\}, \qquad t \to \tilde{\ell}_i^+ + d_k \tag{1.5}$$

where q ($\bar{q}$) is a(n) (anti)quark. This is only kinematically allowed if

$$m_t > m_{\tilde{\ell}i} + m_{d_k}. \tag{1.6}$$

Since, as we shall see, the branching fraction for the B_3 top quark decay is small, we only consider one B_3 decay, for either the top or the antitop quark.

In Ref. [39], single slepton production was considered for the specific case of $\lambda'_{333} \neq 0$. This process is, however, disfavored due to the strict bound on the relevant coupling from neutrino masses, cf. Table I [48]. Thus the work was extended to the couplings λ'_{331} and λ'_{332} [49]. We go beyond this work to include a signal over background analysis. We also present the analytic formula for the cross section, Eq. (2.3), for the first time, and analyze the resulting signatures. We give a detailed phenomenological analysis for the special case λ'_{231} which can be generalized to λ'_{131}.

In Ref. [50], top quark pair production and subsequent top decay via λ'_{i3k} were considered. Off-shell top quark effects were also taken into account. A signal over background analysis was performed for two scenarios. The first scenario assumed maximal stop-scharm mixing. It was pointed out that associated slepton production with slepton masses 150 GeV and 200 GeV can be measured, depending on the magnitude of λ'_{i3k}. The second scenario assumed no flavor violation in the squark sector. Reference [50] claimed that in this regime sleptons with mass of 200 GeV cannot be measured. We go beyond the work of [50]. We show that it is possible to detect associated slepton production even for slepton masses larger than 300 GeV, if λ'_{231} or λ'_{131} is of $\mathcal{O}(0.1)$. We will achieve this with the help of the Compton-like process (1.4).

The outline of this paper is as follows. In Sec. II we calculate the cross section for the production of a charged slepton in association with a top quark, at leading order. In Sec. III we systematically present the possible resulting

signatures at the LHC. In Sec. IV we discuss in detail a case study for the operator $\lambda'_{231} L_2 Q_3 \bar{D}_1$. We study the dominant $t\bar{t}$ and $W^{\pm}$ backgrounds. Using the HERWIG Monte Carlo program [51–53], we devise a set of cuts in order to distinguish the two. We do not include a simulation of the detector. Our conclusions are presented in Sec. V.

II. SINGLE SLEPTON PRODUCTION VIA $L_i Q_3 \bar{D}_k$

A. Partonic cross sections

The spin and color averaged matrix element squared for the Compton-like process Eq. (1.4) is given at leading order by

$$|\bar{M}|^2 = \frac{\pi \lambda'^2_{i3k} \alpha_s C_F |L^{\ell_i}_{1\alpha}|^2}{4} \Bigg\{ \frac{m_t^2 - \hat{t}}{\hat{s}} + \frac{(m^2_{\tilde{\ell}i} - m_t^2)(m^2_{\tilde{\ell}i} - \hat{s} - \hat{t}) - (3m_t^2 - m^2_{\tilde{\ell}i} + \hat{s})(\hat{t} - m^2_{\tilde{\ell}i})}{(\hat{t} - m_t^2)^2} + \frac{2[m_t^2 \hat{s} + (\hat{t} - m^2_{\tilde{\ell}i})(m^2_{\tilde{\ell}i} - m_t^2 - \hat{s})]}{\hat{s}(\hat{t} - m_t^2)} \Bigg\}, \tag{2.1}$$

where α_s is the QCD coupling constant, $C_F = 4/3$ is the quadratic Casimir of $SU(3)_c$, $m_{\tilde{\ell}i}$ is the mass of the slepton, and $L^{\ell_i}_{1\alpha}$ is the relevant matrix element of the left-right slepton mixing matrix. The explicit form as a function of the mixing angle is given, for example, in Ref. [53]. In accordance with the parton model, we have neglected the mass of d_k. We have made use of the partonic Mandelstam variables

$$\hat{s} = (d_k + g)^2 = (t + \tilde{\ell}_i)^2, \tag{2.2a}$$

$$\hat{t} = (d_k - \tilde{\ell}_i)^2 = (g - t)^2, \tag{2.2b}$$

where we denote the particle four-momenta by the particle letter. Integrating over phase space, we obtain the total partonic cross section:

$$\hat{\sigma} = \frac{\lambda'^2_{i3k} \alpha_s C_F |L^{\ell_i}_{1\alpha}|^2}{64 \hat{s}^2} \Bigg\{ \frac{1}{2\hat{s}} [2m_t^2(\hat{t}_+ - \hat{t}_-) - (\hat{t}_+^2 - \hat{t}_-^2)] + (\hat{s} + 2m_t^2) \ln\left(\frac{\rho_-}{\rho_+}\right) + \frac{2m_t^2(m^2_{\tilde{\ell}i} - m_t^2)(\hat{t}_+ - \hat{t}_-)}{\rho_+ \rho_-} + \frac{2(m^4_{\tilde{\ell}i} + m_t^4 - 2m_t^2 m^2_{\tilde{\ell}i} - m^2_{\tilde{\ell}i}\hat{s})}{\hat{s}} \ln\left(\frac{\rho_-}{\rho_+}\right) + \frac{2(\hat{t}_+ - \hat{t}_-)(m^2_{\tilde{\ell}i} - m_t^2 - \hat{s})}{\hat{s}} \Bigg\}, \tag{2.3}$$

where

$$\rho_{\pm} = m_t^2 - \hat{t}_{\pm}, \tag{2.4}$$

$$\hat{t}_{\pm} = m^2_{\tilde{\ell}i} - \tfrac{1}{2}[\hat{s} + m^2_{\tilde{\ell}i} - m_t^2 \mp \lambda^{1/2}(\hat{s}, m^2_{\tilde{\ell}i}, m_t^2)], \tag{2.5}$$

with the phase-space function given by $\lambda(x, y, z) = x^2 + y^2 + z^2 - 2xy - 2xz - 2yz$.

The tree-level partonic matrix element squared for top quark pair production is given, for example, in Ref. [54]. We shall only consider on-shell top quark pair production. The slepton then arises through the decay of a real top quark. In order to obtain the signal rate, we thus also require the partial decay width of the top quark, via the $L_i Q_3 \bar{D}_k$ operator. It is given by

$$\Gamma_{t \to d_k \tilde{\ell}_i^+} = \frac{\lambda'^2_{i3k} |L^{\ell_i}_{1\alpha}|^2}{32\pi m_t} \left(1 + \frac{m_{d_k}^2}{m_t^2} - \frac{m^2_{\tilde{\ell}i}}{m_t^2}\right) \lambda^{1/2}(m_t^2, m_{d_k}^2, m^2_{\tilde{\ell}i}). \tag{2.6}$$

See also Refs. [39,46,53,55,56]. We obtain a branching ratio of 8.2×10^{-4} for the R-parity violating top decay (2.6) with $\lambda'_{i3k} = 0.1$, $m_t = 175$ GeV, top width $\Gamma_t = 1.5$ GeV and $m_{\tilde{\ell}i} = 150$ GeV. We neglect the mass of d_k and set $L^{\ell_i}_{1\alpha} = 1$.

B. Total hadronic cross section

In Fig. 2 (Fig. 3), we show the hadron level cross section at the Tevatron (LHC) for single slepton production in association with a top quark, as a function of the slepton mass including both production mechanisms. We set $\lambda'_{i3k} = 0.1$ and assume it is the only nonvanishing B_3 coupling. We vary the index k and the charge of the final-state slepton, which correspond to different parton density functions (PDFs). Here we use the CTEQ6L1 PDFs [57], corresponding to $\Lambda_5^{\rm LO} = 165$ MeV at the one-loop level of the strong coupling $\alpha_s(\mu_R)$ using $\alpha_s(M_z) = 0.130$. We use the same running α_s to calculate the cross section (2.3). The renormalization, μ_R, and factorization, μ_F, scales are taken to be equal, $\mu_R = \mu_F = m$, where $m \equiv 2m_t$ [$\equiv m_{\tilde{\ell}i} + m_t$] in the case of slepton production via a $t\bar{t}$ pair (1.5) [via the Compton-like process (1.4)]. Furthermore, we set the left-right slepton mixing matrix element $L^{\ell_i}_{1\alpha}$ equal to 1. Results for other values of λ'_{i3k} and mixing matrix elements $L^{\ell_i}_{1\alpha}$ are easily obtained by rescaling according to Eqs. (2.3) and (2.6). The top mass is taken to be 175 GeV and the total (SM) top quark decay width to be 1.5 GeV. We take $m_{d_3} = m_b = 4.5$ GeV, if we have a b quark in the final state and neglect the masses of the d and s quarks.

In both figures, we see a kink in the cross section when $m_{\tilde{\ell}i} = m_t - m_{d_k}$. For smaller slepton masses the top quark pair production mechanism dominates; for larger masses the Compton-like processes dominate, since the slepton can no longer be produced on shell in top decay.

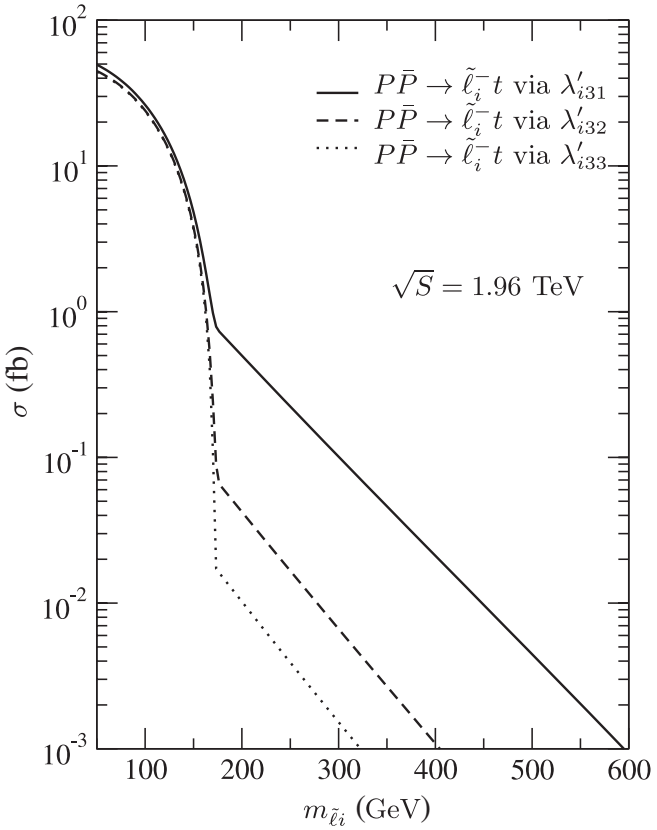

FIG. 2. Single charged slepton production in association with a top quark at the Tevatron. The cross sections for $\tilde{\ell}_i^+ \bar{t}$ production are equal to the cross sections for $\tilde{\ell}_i^- t$ production.

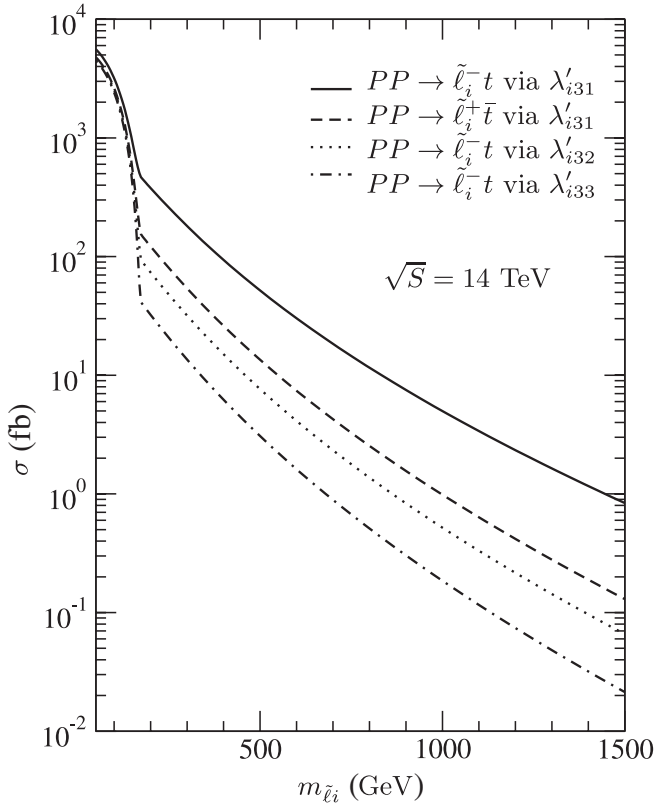

FIG. 3. Same as Fig. 2, but for the LHC. The cross section for $\tilde{\ell}_i^+ \bar{t}$ production via λ'_{i32} (λ'_{i33}) is equal to the cross section for $\tilde{\ell}_i^- t$ production via λ'_{i32} (λ'_{i33}), as it always involves incoming sea quarks.

For comparative discussions later, Fig. 4 (Fig. 5) shows the NLO hadronic cross section for resonant sneutrino production, cf. Eq. (1.3), at the Tevatron (LHC) via $\lambda'_{i3k} = 0.1$, including NLO-QCD corrections [58]. We employ the $\overline{\text{MS}}$ renormalization scheme and the (NLO) CTEQ6M PDFs [57], corresponding to $\Lambda_5^{\overline{\text{MS}}} = 226$ MeV at the two-loop level of $\alpha_s(\mu_R)$ with $\alpha_s(M_z) = 0.118$. The renormalization and factorization scales are taken to be the sneutrino mass, $\mu_R = \mu_F = m_{\tilde{\nu}_i}$.

In Fig. 2, we see that at the Tevatron, even for small slepton masses, $m_{\tilde{\ell}i} = 100$ GeV, we expect only 25 (25) charged slepton events with negative (positive) charge, i.e. $\tilde{\ell}_i^-$ ($\tilde{\ell}_i^+$), for an integrated luminosity of 1 fb^{-1} and the (relatively large) coupling $\lambda'_{i31} = 0.1$. The cross section is dominated by the $t\bar{t}$ pair production (1.5). Only 10% of the above sleptons at the Tevatron are produced by the Compton-like process (1.4). At the Tevatron, the cross section is symmetric in the slepton charge due to the charge symmetry of the incoming state.

As we can see in Fig. 3, we have a significantly larger hadronic cross section at the LHC for a given slepton mass. In particular, for $m_{\tilde{\ell}i} = 100$ GeV and $\lambda'_{i31} = 0.1$ the LHC will produce more than 31 000 (26 000) sleptons $\tilde{\ell}_i^-$ ($\tilde{\ell}_i^+$) for an integrated luminosity of 10 fb^{-1}. Of these sleptons, 27% (11%) are produced via the Compton-like process. For the same coupling and for $m_{\tilde{\nu}_i} = 100$ GeV, we will produce approximately 14 000 sneutrinos at the Tevatron (Fig. 4) for 1 fb^{-1} and 3 800 000 at the LHC (Fig. 5) for 10 fb^{-1}, via the partonic process, Eq. (1.3). Thus, depending on the decays, we might expect this to be the discovery mode, for equal supersymmetric masses. Here we focus on the potential of the charged slepton production cross section.

For heavier charged sleptons, $m_{\tilde{\ell}i} = 800$ GeV, we expect no events at the Tevatron and more than 110 (25) $\tilde{\ell}_i^-$ ($\tilde{\ell}_i^+$) events at the LHC with 10 fb^{-1}. Above the threshold of $m_{\tilde{\ell}i} = m_t - m_{d_k}$, practically all slepton events are produced via the Compton-like process, since the other process only proceeds via off-shell top quarks. The cross section is so small because the parton luminosity is too small at the required high values of the proton/antiproton fractional momenta, $x \gtrsim 0.1$. This situation changes at the LHC, where we probe significantly smaller values, $x < 0.1$, for the same slepton mass. Furthermore, the Tevatron will produce no sneutrinos, for $\lambda'_{i31} = 0.1$, and $m_{\tilde{\nu}i} = 800$ GeV. For the same set of B_3 parameters, the LHC will produce about 3200 sneutrinos for 10 fb^{-1}.

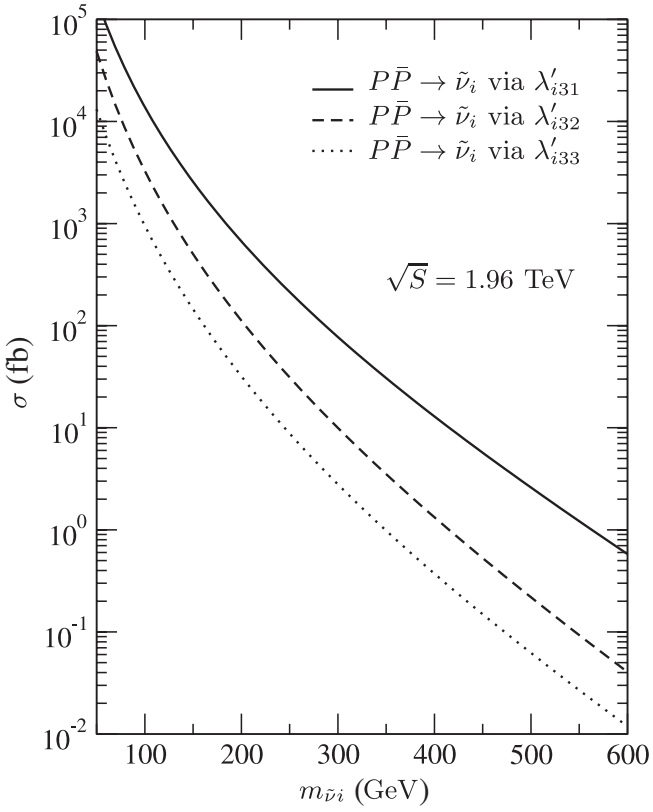

FIG. 4. Single sneutrino production cross section at the Tevatron. The cross sections for $\tilde{\nu}_i^*$ production are equal to the cross sections for $\tilde{\nu}_i$ production.

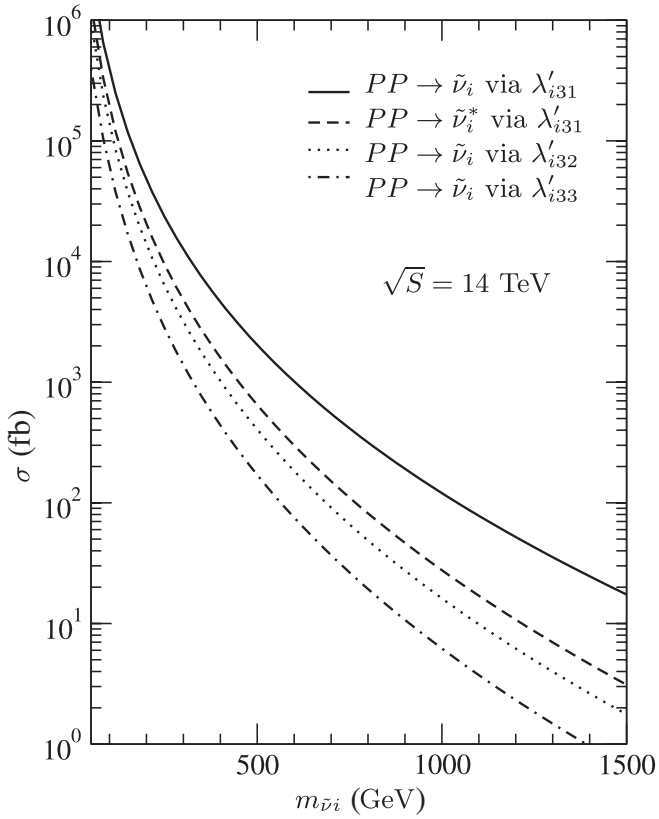

FIG. 5. Same as Fig. 4, but for the LHC. The cross section for $\tilde{\nu}_i^*$ production via λ'_{i32} (λ'_{i33}) is equal to the cross section for $\tilde{\nu}_i$ production via λ'_{i32} (λ'_{i33}), since only initial-state sea quarks are involved.

At the LHC, there is an asymmetry between the hadronic cross sections for $\tilde{\ell}_i^-$ and $\tilde{\ell}_i^+$ production via the $L_i Q_3 \bar{D}_1$ operator ($k = 1$!). This is perhaps not surprising, as the initial state is asymmetric under charge reversal. In the case of the Compton-like process (1.4), the asymmetry is due to the negatively charged slepton being produced by an incoming valence d quark, while the positively charged slepton is produced by a $\bar{d}$ sea quark. The latter has a lower luminosity in the proton. In Sec. IV we will use this asymmetry to separate the B_3 process from the SM background.

In order to estimate the influence of higher order corrections on the production cross section, we vary the renormalization and factorization scales independently between $m/2$ and $2m$. At the Tevatron, Fig. 6, the hadronic cross section for $\tilde{\ell}_i^- t$ production via λ'_{i31} changes by up to 40%. At the LHC, Fig. 7, the scale uncertainties are reduced to approximately 25%. In the domain where $m_{\tilde{\ell}i} < m_t - m_{d_k}$, we have a stronger dependence on the renormalization scale compared to $m_{\tilde{\ell}i} > m_t - m_{d_k}$, because $t\bar{t}$ production is $\mathcal{O}(\alpha_s^2(\mu_r))$. According to Refs. [59,60], NLO-QCD corrections, including a next-to-leading log resummation, increase the $t\bar{t}$ production cross section by approximately 40% (80%) at the Tevatron (LHC).

Because of the large scale uncertainties, a NLO calculation is called for. In the case of nonvanishing λ'_{i33}, the Compton-like process (1.4a) is similar to associated charged Higgs production [39] via the partonic process

$$g + b \to H^- + t, \tag{2.7}$$

with the replacement $\tilde{\ell}_i^- \to H^-$. This process has first been calculated at NLO in QCD in Refs. [61,62]. It was shown that the NLO contributions enhance the total hadronic cross section between 30% and 80%. It was also shown that the perturbative behavior is well under control and that the higher order contributions reduce the scale uncertainties significantly. However, for $\lambda'_{i31(2)}$, the correspondence to the Higgs production process (2.7) at the hadron level no longer holds due to the light quark, i.e. the d quark (s quark), instead of the heavy b quark in the initial state. The parton-level calculation for different couplings λ'_{i3k} is the same. We conclude that, particularly for the case of nonvanishing λ'_{i31}, where the lepton charge asymmetry can be observed at the LHC, a NLO calculation has to be done. It is, however, beyond the scope of this paper.

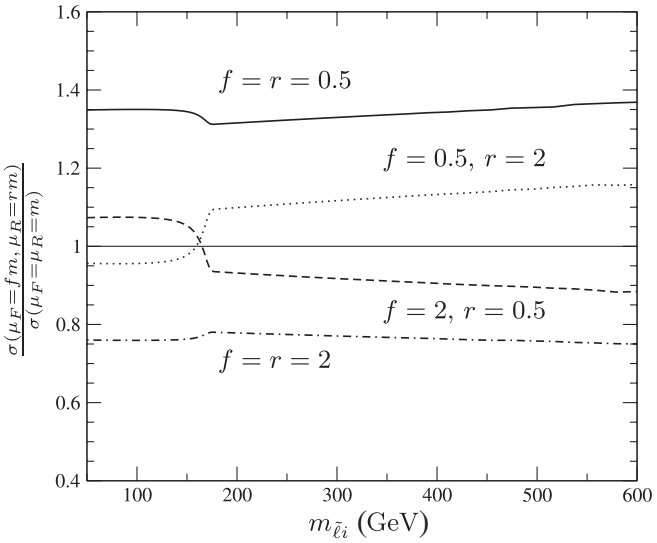

FIG. 6. Factorization scale $\mu_F = f \cdot m$ and renormalization scale $\mu_R = r \cdot m$ dependence of the hadronic $\tilde{\ell}_i^- t$ production cross section via λ'_{i31} at the Tevatron. μ_F and μ_R are independently taken equal to 2 and 0.5 times m, where $m \equiv 2m_t$ [$\equiv m_{\tilde{\ell}i} + m_t$] in the case of slepton production via a $t\bar{t}$ pair, Eq. (1.5) [via the Compton-like process Eq. (1.4)].

The hadronic cross section for single stau, $\tilde{\tau}$, production via a nonvanishing λ'_{333} coupling was also considered by Borzumati *et al.* [39]. There, the $2 \to 2$ processes, Eqs. (1.4), were included, together with the (tree-level) $2 \to 3$ slepton-strahlung processes

$$\left.\begin{matrix} g + g \\ q + \bar{q} \end{matrix}\right\} \to t + \bar{b} + \tilde{\tau}^-, \tag{2.8}$$

which are shown, for $m_{\tilde{\tau}} < m_t - m_b$, to be equivalent to the $2 \to 2$ processes, Eqs. (1.5). The $\bar{b}$ and $\tilde{\tau}^-$ are produced via a virtual top. They employed the CTEQ4L [63] PDFs, and all matrix elements were multiplied by the Cabibbo-Kobayashi-Maskawa (CKM) factor V_{tb}. We have calculated the hadronic cross sections using the same PDFs and the same parameter set [64]. We agree exactly, where single slepton production is dominated by the $t\bar{t}$ process, i.e. for $m_{\tilde{\tau}} < m_t - m_b$. For $m_{\tilde{\tau}} > m_t - m_b$, we underestimate the total cross section at the Tevatron by 20% for $m_{\tilde{\tau}} = 300$ GeV and by a factor of roughly 2 for $m_{\tilde{\tau}} = 200$ GeV, compared to Ref. [39]. In this region the above $2 \to 3$ processes, where the slepton is produced by a quark-antiquark pair, can give the main contribution compared to the $gb \to \tilde{\tau} t$ partonic process, where a gluon and/or sea quark is needed with a large Bjorken x. However, in this region where there are large discrepancies, practically no sleptons are produced at the Tevatron. Our prediction for the LHC differs by +30% for $m_{\tilde{\tau}} > m_t - m_b$.

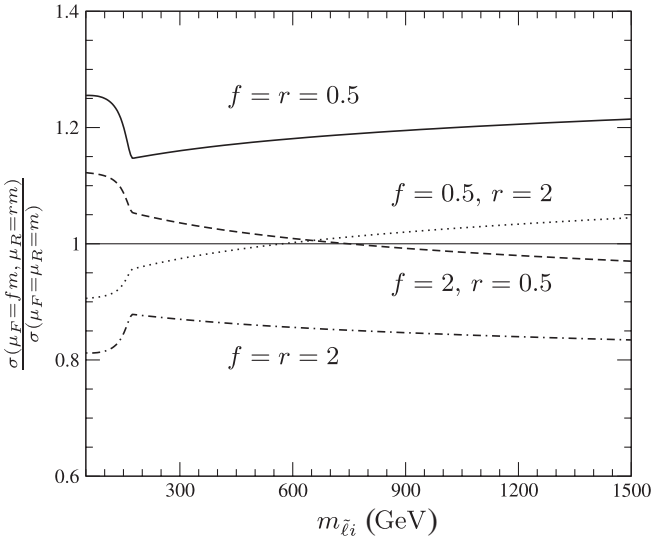

FIG. 7. Same as Fig. 6 but for the LHC.

Borzumati *et al.* extended their analysis to the λ'_{332} and λ'_{331} couplings [65]. They presented the results for the $2 \to 2$ process (1.4) and the $2 \to 3$ process (2.8) separately. For $m_{\tilde{\tau}} < m_t - m_{d_k}$, we agree exactly at the Tevatron as well as at the LHC. For $m_{\tilde{\tau}} > m_t - m_{d_k}$, our predictions coincide exactly with their cross section predictions for the $2 \to 2$ process. Furthermore, it is shown in [65] that for $m_{\tilde{\tau}} > m_t - m_{d_k}$, the $2 \to 3$ contributions are small or even negligible. At the Tevatron, the $2 \to 3$ process contributes roughly 35% (5%) to the total hadronic cross section for $\lambda'_{332} \neq 0$ ($\lambda'_{331} \neq 0$). At the LHC these contributions are 25% (5%). The reason is that the cross sections induced by the $2 \to 3$ process have similar sizes for any value of k. But the $2 \to 2$ process for $\lambda'_{332} \neq 0$ ($\lambda'_{331} \neq 0$) is enhanced by a factor of 5 ($\gtrsim 10$) due to an s quark (valence d quark) in the initial state.

We conclude that our LO approximation is valid in the phenomenologically relevant region, where one is able to produce a single slepton in association with a top quark. We have not included the $2 \to 3$ processes as they are formally higher order. Furthermore, the essential ingredient in our phenomenological analysis below is the lepton charge asymmetry due to a nonvanishing λ'_{i31} coupling. The $2 \to 3$ processes do not contribute, as their initial states are charge symmetric and their contributions to the hadronic cross section are only 5%.

TABLE II. Hadronic cross section predictions for $\tilde{\ell}_i^- t$ ($\tilde{\ell}_i^+ t$) production via $\lambda'_{i31} = 0.1$ at the Tevatron ($\sqrt{S} = 1.96$ GeV) and the LHC ($\sqrt{S} = 14$ GeV). Results are presented for the CTEQ6L1 [57] PDF parametrization.

	Tevatron	LHC
$m_{\tilde{\ell}i} = 100$ GeV	25.5 fb	3180 (2620) fb
$m_{\tilde{\ell}i} = 250$ GeV	2.10×10^{-1} fb	259 (80.0) fb
$m_{\tilde{\ell}i} = 800$ GeV	2.86×10^{-5} fb	11.6 (2.54) fb

We end this section by presenting in Table II selected cross section predictions for slepton production with $m_{\tilde{\ell}_i} = 100$ GeV, $m_{\tilde{\ell}_i} = 250$ GeV, and $m_{\tilde{\ell}_i} = 800$ GeV at the Tevatron and the LHC via $\lambda'_{i31} = 0.1$.

III. POSSIBLE LHC SIGNATURES

Apart from the B_3 process, the sleptons and sneutrinos can decay through gauge interactions. Neglecting mixing between left- and right-handed sleptons, the possible tree-level decays are

$$\tilde{\ell}_i^- \to \begin{cases} \bar{t} d_k \\ \ell_i^- \tilde{\chi}_m^0 \\ \nu_i \tilde{\chi}_n^-, \end{cases} \qquad \tilde{\nu}_i \to \begin{cases} \bar{b} d_k \\ \nu_i \tilde{\chi}_m^0 \\ \ell_i^- \tilde{\chi}_n^+. \end{cases} \tag{3.1}$$

The branching ratios depend on the masses of the sparticles, the admixtures of the gauginos, and on the size of the λ'_{i3k} coupling. We shall first assume that the lightest neutralino, $\tilde{\chi}_1^0$, is the LSP. Possible decay modes via the λ'_{i3k} interaction are

$$\tilde{\chi}_1^0 \xrightarrow{\lambda'} \begin{cases} \ell_i^+ \bar{t} d_k \\ \ell_i^- t \bar{d}_k, \end{cases} \qquad \tilde{\chi}_1^0 \xrightarrow{\lambda'} \begin{cases} \bar{\nu}_i \bar{b} d_k \\ \nu_i b \bar{d}_k. \end{cases} \tag{3.2}$$

Here the branching ratios depend mainly on the admixture of the lightest neutralino. The heavier neutralinos $\tilde{\chi}_{2,3,4}^0$ and the charginos $\tilde{\chi}_{1,2}^+$ dominantly decay into lighter gauginos via gauge interactions, as in the P_6 minimal supersymmetric standard model. We have neglected the decay $\tilde{\chi}_1^0 \to \nu\gamma$ [66], which is suppressed except for very light neutralino masses [67].

In SUSY scenarios, where the slepton (sneutrino) mass is of the order of a few hundred GeV, the slepton (sneutrino) will decay dominantly into the lightest neutralino and a lepton (neutrino). However, significant chargino decay modes are also possible, if they are kinematically accessible. Furthermore, decay chains involving a top quark in the final state are either phase-space suppressed or kinematically forbidden, unless the slepton is very heavy. This affects the neutralino decays (3.2) involving charged leptons. Therefore, the dominant hadron collider signatures of single slepton production in association with a top quark are

$$g d_k \to \tilde{\ell}_i^- t \to \ell_i^- \tilde{\chi}_1^0 t \to \begin{cases} \ell_i^- (\bar{\nu}_i \bar{b} d_k)[b W^+] \\ \ell_i^- (\nu_i b \bar{d}_k)[b W^+]. \end{cases} \tag{3.3}$$

In parentheses are the neutralino LSP decay products (3.2); the particles in brackets arise from the top quark decay. As mentioned before, for $k = 1$ there is an asymmetry between the number of positively and negatively charged leptons $\ell_i^\pm$ at the LHC.

The dominant signatures for a resonantly produced single sneutrino are

$$\bar{b} d_k \to \tilde{\nu}_i \to \begin{cases} \bar{b} d_k \\ \nu_i (\bar{\nu}_i \bar{b} d_k) \\ \nu_i (\nu_i b \bar{d}_k). \end{cases} \tag{3.4}$$

Again the neutralino decay products are in parentheses. Although the sneutrino production cross section at the LHC (Fig. 5) is up to 2 orders of magnitude larger than the slepton plus top quark cross section (Fig. 3), the event signature (3.4) is much harder to extract above the SM background. It involves only two jets and possibly some missing transverse energy. It therefore suffers from a large QCD background. However, if the sneutrino decays into charginos and heavier neutralinos are possible (3.1), we can have (additional) charged leptons in the final state.

We now consider SUSY scenarios, where the scalar tau (stau) is the LSP instead of the lightest neutralino [18,26,68]. In this scenario the lightest neutralino dominantly decays into a tau and the stau LSP, $\tilde{\chi}_1^0 \to \tilde{\tau}_1^\pm \tau^\mp$. For $i = 1, 2$, the stau will dominantly decay into a tau and a virtual neutralino, leading to a four-body decay of the stau LSP [26]. The signatures for a stau LSP are

$$g d_k \to \tilde{\ell}_i^- t \to \begin{cases} \ell_i^- \tau^\pm (\tau^\mp \bar{\nu}_i \bar{b} d_k)[b W^+] \\ \ell_i^- \tau^\pm (\tau^\mp \nu_i b \bar{d}_k)[b W^+]. \end{cases} \tag{3.5}$$

The particles in parentheses are now the stau LSP decay products and the particles in brackets are from the top quark decay. The difference between the final states in Eqs. (3.3) and (3.5) is that, for a stau LSP, the event is accompanied by an additional pair of taus compared to scenarios with a neutralino LSP. We find the same behavior for the sneutrino decay chains. It is therefore easier to distinguish the signal from the background in stau LSP scenarios as long as one is able to reconstruct the tau pair in the final state.

Note that for $i = 3$ the two-body stau decay is kinematically suppressed, or forbidden, due to the large top quark mass. The stau LSP will, in this case, decay via a virtual top quark. Furthermore, we can produce heavy staus, $\tilde{\tau}_2$, as well as light staus, $\tilde{\tau}_1$, due to left-right mixing in the stau sector. In this case the signatures are

$$g d_k \to \tilde{\tau}_2^- t \to \begin{cases} \tau^- \tau^+ (\bar{b} d_k W^-)[b W^+] \\ \tau^- \tau^- (b \bar{d}_k W^+)[b W^+] \\ Z^0/h^0 (\bar{b} d_k W^-)[b W^+] \end{cases} \tag{3.6}$$

and

$$g d_k \to \tilde{\tau}_1^- t \to (\bar{b} d_k W^-)[b W^+]. \tag{3.7}$$

The particles in parentheses are the stau LSP decay products and those in brackets are from the top quark decay. We see in Eq. (3.6) that one of the $\tilde{\tau}_2$ decay chains involves like-sign tau events. This can help to distinguish signal from background, although poor tau identification could limit this possibility.

TABLE III. Relevant branching ratios for SPS1a′ for different couplings λ'_{231}.

λ'_{231}	0	0.1	0.2	0.3	0.4
$\mathrm{Br}(\tilde{\mu}^- \to \bar{t} + d)$	0.0%	2.2%	8.4%	17.1%	26.8%
$\mathrm{Br}(\tilde{\mu}^- \to \mu^- + \tilde{\chi}_1^0)$	90.9%	88.9%	83.3%	75.4%	66.5%
$\mathrm{Br}(\tilde{\mu}^- \to \mu^- + \tilde{\chi}_2^0)$	3.2%	3.1%	2.9%	2.6%	2.3%
$\mathrm{Br}(\tilde{\mu}^- \to \nu_\mu + \tilde{\chi}_1^-)$	5.9%	5.8%	5.4%	4.9%	4.3%

IV. NUMERICAL STUDY FOR $\lambda'_{231} \neq 0$ AND A $\tilde{\chi}_1^0$ LSP

A. The scenario and basic cuts

We now perform an explicit numerical study of single associated slepton production. We focus on the more difficult case of a neutralino LSP and restrict ourselves to $\lambda'_{231} \neq 0$, as the dominant B_3 coupling. We assume that similar results can be obtained for $\lambda'_{131} \neq 0$. A central analysis criterion will be the lepton charge asymmetry of the final state.

According to Eq. (3.3), the final-state signature to examine is

$$\tilde{\ell}_L^{\mp} + t \to \ell^{\mp} + (b + d + \nu) + [b + W^{\pm}], \qquad (4.1)$$

with the $W^{\pm}$ decaying hadronically. We thus have one charged lepton, some missing p_T, and five jets, where two are b-quark jets. In our specific scenario, the charged lepton is a muon.

The main background for this process is $t\bar{t} + j$ production (which has recently been calculated at NLO [69]) followed by the semileptonic decay of one of the top quarks. The second background we examine is $b\bar{b} + W^{\pm}$ + jets production followed by the leptonic decay of the W boson.

For our simulation, we assume an SPS1a′ similar scenario [70]. We take the SPS1a′ spectrum and couplings and add one B_3 coupling, λ'_{231}. The relevant SPS1a′ masses are

$$m_{\tilde{\ell}_L^{\pm}} = 190 \text{ GeV}; \qquad m_{\tilde{\nu}_\mu} = 173 \text{ GeV}; \qquad (4.2a)$$

$$m_{\tilde{\chi}_1^0} = 98 \text{ GeV}; \qquad m_{\tilde{\chi}_2^0} = 184 \text{ GeV}; \qquad (4.2b)$$

$$m_{\tilde{\chi}_1^{\pm}} = 183 \text{ GeV}. \qquad (4.2c)$$

All the charged slepton decays of Eq. (3.1) are therefore kinematically possible. The corresponding branching ratios are given in Table III for various couplings λ'_{231}. Note that kinematically the sneutrino can only decay via the neutralino or via the λ'_{231} coupling. The potential signature would then be two jets possibly with some missing energy; cf. Eq. (3.4).

For the simulation of the single slepton plus top quark signal, we have written our own Monte Carlo program using the Les Houches accord [71] and linked this to HERWIG6.5 [51,52,72]. The averaging of the color flow in the s- and t-channel single slepton production diagrams is implemented by the method developed in Ref. [73]. The supersymmetric particle spectra are produced with SOFTSUSY [74]. The $t\bar{t}$ background is simulated using the MC@NLO program [75,76]. The $b\bar{b} + W^{\pm}$ + jets background is simulated by using MADEVENT [77] to generate a sample of $b\bar{b} + W^{\pm} + 2$ jet events which are then showered and hadronized using HERWIG6.5. We use the CTEQ61 parton distribution functions [57]. The top quark mass is set to $m_t = 175$ GeV.

Since our signature is very similar to the final state and distributions of $t\bar{t} + j$ production followed by the semileptonic decay, we use the standard set of CMS cuts for $t\bar{t}$ production followed by the semileptonic decay, given in Ref. [78], and require an additional jet. This set of cuts leaves the large semileptonic $t\bar{t} + j$ production, for which the cuts are designed, and fewer $b\bar{b} + W^{\pm}$ + jets events as backgrounds for the signal process. The precise cuts are summarized below.

The main difference between the semileptonically decaying top pair and our signal is the p_T distribution of the lepton stemming from the slepton compared to the one from the $W^{\pm}$ from one of the top decays. We therefore

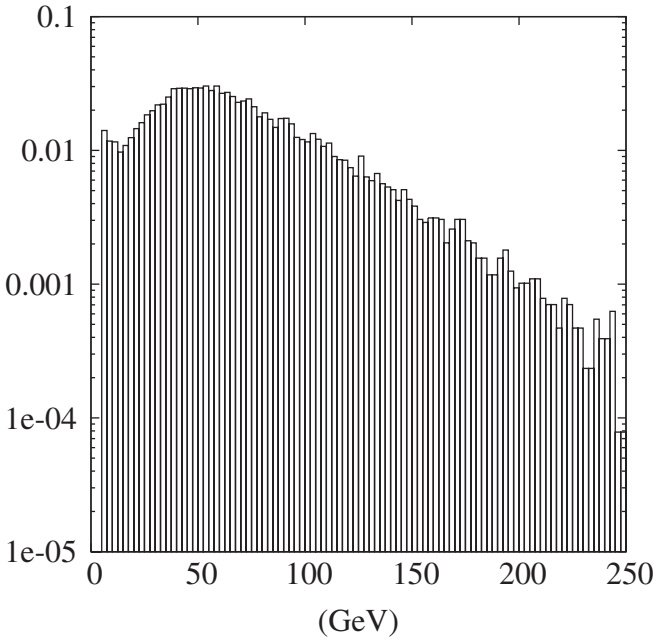

FIG. 8. Relative p_T distribution of the final-state signal $\ell^{\pm}$ at the LHC for SPS1a′, employing only the isolation cut on the lepton.

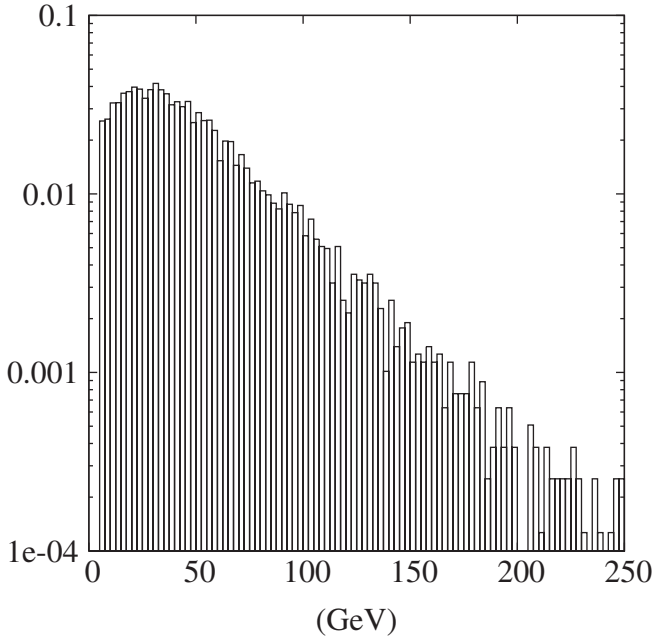

FIG. 9. Relative p_T distribution of the final-state $\ell^{\pm}$ from $t\bar{t}+j$ background at the LHC, employing only the isolation cut on the lepton.

compare in Figs. 8 and 9 the p_T distributions of the leptons arising from the signal and the $t\bar{t}+j$ background processes, respectively. We see that the p_T of the signal leptons has a peak around 50 GeV. This peak corresponds to the mass difference between the slepton and the neutralino with the energy carried away by the lepton having been subtracted. The background lepton distribution peaks at 25 GeV and then falls more steeply than the signal distribution for increasing p_T. We thus harden the CMS semileptonic $t\bar{t}$ cut for the isolated observed lepton from $p_T \geq 20$ GeV to $p_T \geq 35$ GeV.

In addition to the charged lepton in the final state, we require two tagged b jets, as well as two further jets. Thus, the employed cuts are as follows:

(i) One isolated lepton with pseudorapidity $\eta < 2.4$, $p_T > 35$ GeV. The isolation cut requires less than 2 GeV of transverse energy in a cone of radius 0.4 around the lepton direction.

(ii) Two isolated b jets and two non-b jets, with pseudorapidity $\eta < 2.4$, $p_T > 30$ GeV.

The jets are defined using PXCONE [79] which uses the midpoint between two particles as a seed in addition to the particles themselves to improve the infrared behavior of the algorithm. A cone radius of 0.5 was used to define the jets. For the bottom and charm quarks produced in the perturbative stage of the event, the nearest jet in (η, ϕ) is considered to have been produced by that quark if the distance in (η, ϕ) was less than 0.2. We employ a b-tagging probability of 0.6 and the probability for mistagging a c quark or light quark as a b quark of 0.05 and 0.02, respectively.

For the signal, we simulated 10^5 events. Employing all cuts, including $p_T(\ell^{\pm}) \geq 35$ GeV, we have 5×10^3 surviving ℓ^- events and 1.7×10^3 surviving ℓ^+ events. For the $b\bar{b} + W^{\pm} +$ jets background we simulated 10^6 events for both W^- and W^+ production. After all cuts we are left with 2.9×10^4 ℓ^- and 3.0×10^4 ℓ^+ events, respectively. There were 10^7 $t\bar{t}+j$ events simulated resulting in 1.35×10^5 events for ℓ^- production and 1.36×10^5 events for ℓ^+ production. This is summarized in Table IV.

For the simulated signal, we set $\lambda'_{231} = 0.053$. In the following, we will estimate the signal for other values of λ'_{231} by taking into account the λ'^2_{231} dependence of the cross section. We also employ the λ'_{231} dependence of the $\tilde{\mu}^- \rightarrow \mu^- + \tilde{\chi}^0_1$ branching ratio.

B. Lepton charge asymmetry

In order to distinguish the signal from the background at the LHC after these cuts, we propose as the decisive observable the lepton charge asymmetry

$$\mathcal{A}_{\ell^{\pm}} \equiv \frac{N_{\ell^+} - N_{\ell^-}}{N_{\ell^+} + N_{\ell^-}}. \tag{4.3}$$

Here N_{ℓ^+} and N_{ℓ^-} are the number of events with a positively or negatively charged lepton, respectively. In Fig. 3, we can see the separate signal cross sections for ℓ^+ and ℓ^- production at the LHC. For $m_{\tilde{\ell}^{\pm}_L} > m_t - m_d$, the ℓ^- cross section is significantly larger. This is due to the fact that the d-quark PDF luminosity is significantly larger than that of the $\bar{d}$ quark for $x \gtrsim 10^{-2}$.

We would expect the lepton charge asymmetry to be zero for the $t\bar{t}+j$ background, as we have an equal number of top quarks and antitop quarks. For the background

TABLE IV. Results of simulating SPS1a′ with cuts given in the text. The number of leptons and the expected event rates are after cuts.

	Simulated	ℓ^- events after cuts	ℓ^+ events after cuts	Events/pb^{-1}
Signal	99 900	5042	1664	0.0108
$W^- + b\bar{b} +$ jets bg	994 000	28 600	0	0.0431
$W^+ + b\bar{b} +$ jets bg	993 500	0	29 700	0.0625
$t\bar{t} +$ 1j bg	9 990 500	135 330	136 360	22.00

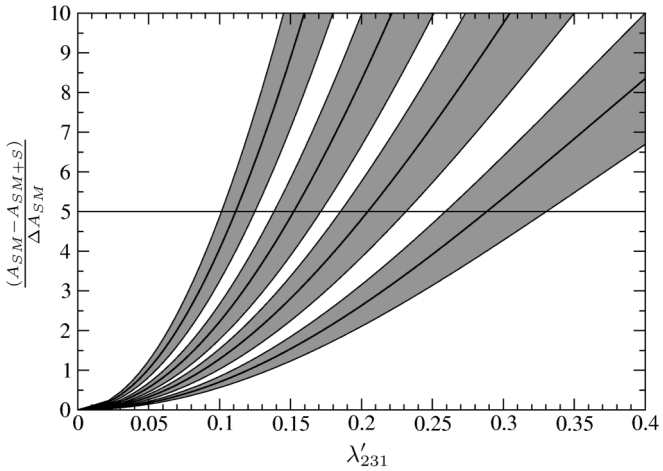

FIG. 10. Significance at the LHC as a function of λ'_{231} for SPS1a′ with lepton $p_T \geq 35$ GeV. We show the significance for an integrated luminosity of 30 fb^{-1} (lower curve), 100 fb^{-1}, 300 fb^{-1}, and 1000 fb^{-1}, respectively. Furthermore, we varied the signal cross section by $\pm 20\%$ (gray region).

process $b\bar{b} + W^{\pm}$ + jets, we expect a positive asymmetry, since the (valence) u-quark luminosity is significantly larger than the (valence) d-quark luminosity in the proton. For the signal, as we have seen, we expect a negative asymmetry.

However, in general, inclusive $t\bar{t}$ production has a charge asymmetry in the final state at the LHC. It has been shown to be in the range $[-0.025\%; 0]$, if the detector has a symmetric acceptance in the rapidity range $[-y_0; y_0]$. For $y_0 \to \infty(0)$ the asymmetry goes to $0\,(-0.025\%)$ [80–82]. This stems from the asymmetry in $q\bar{q}$-induced $t\bar{t}$ production, which in turn is due to the interference of C-odd and C-even modes, where C is the charge conjugation operator. In the following, we will neglect this small asymmetry because the statistical fluctuations lead to an even larger asymmetry. The number of $\ell^{\pm}$ events in Table IV for the $t\bar{t} + j$ background are consistent with a lepton charge asymmetry of zero within two sigma.

In Fig. 10, we show the significance, Σ, of the signal for the SPS1a′ spectrum as a function of λ'_{231}, where

$$\Sigma \equiv \frac{(A_{\mathrm{SM}} - A_{\mathrm{SM}+S})}{\Delta A_{\mathrm{SM}}}. \tag{4.4}$$

Here A_{SM} is the SM lepton charge asymmetry. $A_{\mathrm{SM}+S}$ is the asymmetry for the signal and the SM background combined. ΔA_{SM} is the error of the SM asymmetry prediction assuming purely statistical errors for the number of positively and negatively charged leptons for each process separately, i.e. $\sqrt{N_{\ell+}}$ and $\sqrt{N_{\ell-}}$. The significance is shown for integrated luminosities at the LHC of 30 fb^{-1} (lower curves), 100 fb^{-1}, 300 fb^{-1}, and 1000 fb^{-1}, respectively. We vary the cross section by $\pm 20\%$ (gray region) to show possible effects due to higher order corrections for the signal (cf. Fig. 7).

In Fig. 10, we see that for 30 fb^{-1} we can probe couplings down to about 0.3 for the SPS1a′ spectrum. In the SPS1a′ spectrum the squark mass is 544 GeV, and thus the experimental bound is $\lambda'_{231} < 1.0$; cf. Table I. For 300 fb^{-1} we can probe couplings down to about 0.15. In the extreme case of 1000 fb^{-1}, this improves to about $\lambda'_{231} = 0.1$.

We have repeated the above analysis for the parameter set SPS1b [83]. Here we have the following masses:

$$m_{\tilde{\mu}_L} = 342 \text{ GeV}; \qquad m_{\tilde{\nu}_\mu} = 333 \text{ GeV}; \tag{4.5a}$$

$$m_{\tilde{\chi}_1^0} = 163 \text{ GeV}; \qquad m_{\tilde{\chi}_2^0} = 306 \text{ GeV}; \tag{4.5b}$$

$$m_{\tilde{\chi}_1^{\pm}} = 306 \text{ GeV}. \tag{4.5c}$$

We show the branching ratios for different λ'_{231} in Table V. We see that the B_3 decay into a d quark and a top quark is the dominant decay for large λ'_{231}, i.e. $\lambda'_{231} > 0.19$. One might thus consider an analysis based on this decay mode. However, the signature is $t\bar{t} + j$, which has a very large background. We thus continue to consider the neutralino decay mode. The significance will then approach a constant value for a constant luminosity and large λ'_{231}, because the cross section and the B_3 decay both scale with λ'^2_{231}. Furthermore, the slepton mass is now significantly larger, but so is the lightest neutralino mass. The mass difference, however, has grown, leading to significantly higher charged lepton p_T's compared to SPS1a′; cf. Fig. 8. We thus impose the stricter cut on the lepton transverse momentum,

$$p_T(\ell^{\pm}) \geq 70 \text{ GeV}. \tag{4.6}$$

The results are shown in Fig. 11. In this case, for the relatively low integrated luminosity of 30 fb^{-1}, we have no chance of observing the signal via the lepton asymmetry; the neutralino branching fraction is too small to have enough events. In fact, it is only for the extremely high integrated luminosity of 1000 fb^{-1} that we have a significant sensitivity range, down to about $\lambda'_{231} = 0.2$.

TABLE V. Relevant branching ratios for SPS1b for different couplings λ'_{231}.

λ'_{231}	0	0.1	0.2	0.3	0.4
$\mathrm{Br}(\tilde{\mu}^- \to \bar{t} + d)$	0.0%	22.0%	53.0%	71.8%	81.9%
$\mathrm{Br}(\tilde{\mu}^- \to \mu^- + \tilde{\chi}_1^0)$	60.9%	47.5%	28.6%	17.2%	11.0%
$\mathrm{Br}(\tilde{\mu}^- \to \mu^- + \tilde{\chi}_2^0)$	13.8%	10.8%	6.5%	3.9%	2.5%
$\mathrm{Br}(\tilde{\mu}^- \to \nu_\mu + \tilde{\chi}_1^-)$	25.3%	19.7%	11.9%	7.1%	4.6%

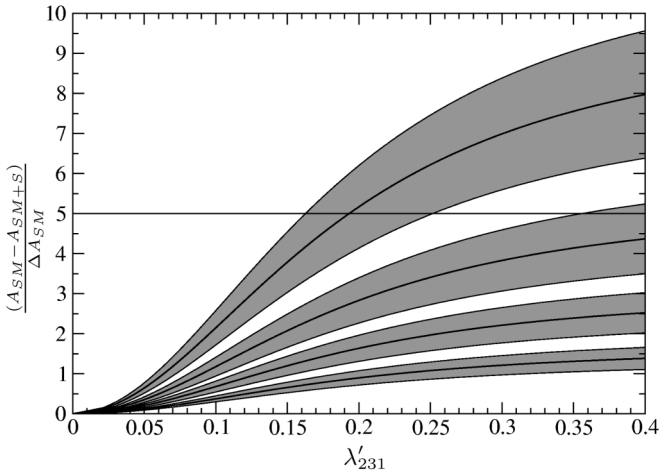

FIG. 11. Same as for Fig. 10, but for the parameter set SPS1b with lepton $p_T \geq 70$ GeV.

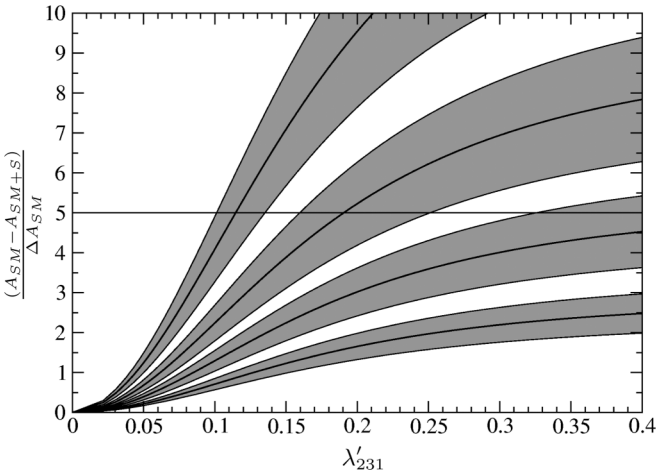

FIG. 12. Same as for Fig. 10, but for the high-p_T scenario and with lepton $p_T \geq 120$ GeV. The scenario is described in the text.

In order to see what can be probed at the LHC, we have chosen as a third example a mass spectrum which optimizes our signal. For this, we considered a modified SPS1b spectrum, where we first lowered the mass of the lightest neutralino to

$$m_{\tilde{\chi}_1^0} = 80 \text{ GeV}, \tag{4.7}$$

in order to obtain a larger mass difference between the smuon and the lightest neutralino. We can then harden the p_T cut to

$$p_T(\ell^\pm) \geq 120 \text{ GeV}. \tag{4.8}$$

This leads to a better signal-to-background ratio compared to SPS1b. Second, we increased the masses of $\tilde{\chi}_2^0$ and $\tilde{\chi}_1^\pm$ to

$$m_{\tilde{\chi}_2^0} = m_{\tilde{\chi}_1^\pm} = 450 \text{ GeV}. \tag{4.9}$$

This increases the $\tilde{\mu}^- \to \mu^- + \tilde{\chi}_1^0$ branching ratio compared to SPS1b, because decays into heavier neutralinos and into charginos are now kinematically forbidden. We show the relevant branching ratios for different λ'_{231} in Table VI. We refer to this scenario as the high-p_T scenario. The resulting significance for the high-p_T scenario is shown in Fig. 12.

As can be seen, for an integrated luminosity of 30 fb^{-1} we still have no sensitivity in λ'_{231}. But now for an integrated luminosity of 300 fb^{-1}, we can probe couplings down to 0.19, well below the experimental bound of 1.5 (cf. Table I), where now $m_{\tilde{b}_L} = 830$ GeV in SPS1b. For an integrated luminosity of 1000 fb^{-1} we can probe couplings down to 0.11.

The influence of systematic errors in the background cross section on our sensitivity is small. Varying the $t\bar{t} + j$ cross section by $+10\%$ (-10%) changes the asymmetry by roughly -9% ($+11\%$). Varying the $b\bar{b} + W^\pm +$ jets cross section by $\pm 10\%$ only effects the asymmetry by $\mp 1.6\%$ for SPS1a$'$ with $\lambda'_{231} = 0.3$ and by $\mp 1.2\%$ for the high-p_T scenario with $\lambda'_{231} = 0.3$. Yet, detector effects resulting in an error on the observed charge asymmetry are a problem. Misalignment in the detector can lead to a difference in the p_T measurement of positive and negative leptons, respectively. This will lead to an observed, effective charge asymmetry after a cut on the lepton p_T [84]. An analysis of this must be performed by the experimentalists and is well beyond the scope of this paper.

For SPS1a$'$ with $\lambda'_{231} = 0.3$, a simulated detector based charge asymmetry of 0.66% leads to an asymmetry of the $t\bar{t}$ background of the same size as that of the signal. For the special case chosen with high-p_T leptons in the final state, i.e. the high-p_T scenario with $\lambda'_{231} = 0.3$, a simulated asymmetry of 0.89% would lead to the same effect. Therefore, a higher p_T cut is less sensitive to systematic errors, due to the high-p_T cut effecting the $t\bar{t}$ background.

V. SUMMARY AND CONCLUSION

Supersymmetry with the discrete symmetry baryon triality (B_3) leads to different signatures at (hadron) col-

TABLE VI. Relevant branching ratios for the high-p_T scenario for different couplings λ'_{231}. The scenario is described in the text.

λ'_{231}	0	0.1	0.2	0.3	0.4
Br($\tilde{\mu}^- \to \bar{t} + d$)	0.0%	23.7%	55.4%	73.6%	83.2%
Br($\tilde{\mu}^- \to \mu^- + \tilde{\chi}_1^0$)	100%	76.3%	44.6%	26.4%	16.8%

liders than conventional, proton hexality (or R-parity) conserving supersymmetry. In this paper, we have investigated single charged slepton production due to the B_3 couplings λ'_{i3k}. These couplings are special, because for resonant charged slepton production they require an incoming top quark, which is not available. Instead, single charged slepton production must proceed via associated production with a final-state top quark. In Sec. II, we have computed the cross section for the Tevatron and the LHC assuming $\lambda'_{i3k} = 0.1$. At the Tevatron we obtain a sizable cross section only for slepton masses below about 200 GeV. At the LHC we have a sizable cross section, greater than about 10 fb, up to about 800 GeV in slepton mass; cf. Fig. 3. It should be kept in mind that the resonant sneutrino production via the same coupling is substantially larger; see Figs. 4 and 5. However, the signature is not necessarily as promising, depending on the nature of the LSP and the dominant sneutrino decay mode. We furthermore showed that the QCD scale uncertainties in the predictions for the associated charged slepton production cross sections are quite large (see Fig. 6 and 7), and therefore a NLO calculation is called for in the future.

Next we classified the possible signatures of associated slepton production with a top quark at the LHC for a neutralino or a stau LSP. We found several promising cases. In Sec. IV, we then analyzed the specific case of a dominant λ'_{231} or λ'_{131} coupling and a neutralino LSP. As the decisive observable, we propose the lepton charge asymmetry at the LHC, which stems from the different parton luminosities involved. We then analyzed the SM background in detail, which stems mainly from $t\bar{t} + j$ production, followed by the leptonic decays of one of the top quarks. We proposed a set of cuts and showed that slepton masses up to 350 GeV can be explored at the LHC depending on the scenario; see Figs. 10–12.

ACKNOWLEDGMENTS

We thank Sebastian Fleischmann, Nicolas Möser, and Jan Schumacher for helpful discussions about the ATLAS detector. We thank Olaf Kittel for reading parts of the manuscript. M. B. thanks the IPPP, Durham, for warm hospitality offered during various stages of this paper. S. G. thanks the Deutsche Telekom Stiftung and the Bonn-Cologne Graduate School for financial support. M. B. and H. D. received financial support from BMBF Grant No. 05 HT6PDA "Rekonstruktion von Parametern der supersymmetrischen Erweiterungen des Standardmodells am LHC."

[1] J. Wess and B. Zumino, Nucl. Phys. **B70**, 39 (1974); For reviews of the supersymmetric standard model, see Refs. [5,85–88].
[2] S. L. Glashow, Nucl. Phys. **22**, 579 (1961); S. Weinberg, Phys. Rev. Lett. **19**, 1264 (1967).
[3] E. Gildener, Phys. Rev. D **14**, 1667 (1976); M. Veltman, Acta Phys. Pol. B **12**, 437 (1981); N. Sakai, Z. Phys. C **11**, 153 (1981); E. Witten, Nucl. Phys. **B188**, 513 (1981).
[4] W. Armstrong *et al.* (ATLAS Collaboration), Technical Proposal No. CERN-LHCC-94-43, 1994; CMS Collaboration, Technical Proposal No. CERN-LHCC-96-45, 1996.
[5] See the discussion in M. Drees, arXiv:hep-ph/9611409.
[6] N. Sakai and T. Yanagida, Nucl. Phys. **B197**, 533 (1982); S. Weinberg, Phys. Rev. D **26**, 287 (1982).
[7] H. K. Dreiner, arXiv:hep-ph/9707435.
[8] J. L. Goity and M. Sher, Phys. Lett. B **346**, 69 (1995); **385**, 500(E) (1996); A. Y. Smirnov and F. Vissani, Phys. Lett. B **380**, 317 (1996); Nucl. Phys. **B460**, 37 (1996).
[9] G. Farrar and P. Fayet, Phys. Lett. **76B**, 575 (1978).
[10] H. K. Dreiner, C. Luhn, and M. Thormeier, Phys. Rev. D **73**, 075007 (2006).
[11] L. E. Ibanez and G. G. Ross, Nucl. Phys. **B368**, 3 (1992).
[12] L. E. Ibanez and G. G. Ross, Phys. Lett. B **260**, 291 (1991).
[13] H. Dreiner, C. Luhn, H. Murayama, and M. Thormeier, Nucl. Phys. **B774**, 127 (2007).
[14] L. Hall and M. Suzuki, Nucl. Phys. **B231**, 419 (1984).
[15] R. Hempfling, Nucl. Phys. **B478**, 3 (1996).
[16] F. Borzumati, Y. Grossman, E. Nardi, and Y. Nir, Phys. Lett. B **384**, 123 (1996).
[17] M. Hirsch, M. A. Diaz, W. Porod, J. Romao, and J. Valle, Phys. Rev. D **62**, 113008 (2000); **65**, 119901(E) (2002).
[18] B. C. Allanach, A. Dedes, and H. K. Dreiner, Phys. Rev. D **69**, 115002 (2004).
[19] B. C. Allanach and C. H. Kom, J. High Energy Phys. 04 (2008) 081.
[20] H. K. Dreiner, J. Soo Kim, and M. Thormeier, arXiv: 0711.4315.
[21] B. T. Cleveland *et al.*, Astrophys. J. **496**, 505 (1998); Y. Fukuda *et al.*, Phys. Rev. Lett. **82**, 2644 (1999); **81**, 1158 (1998); **81**, 4279(E) (1998); Q. R. Ahmad *et al.*, Phys. Rev. Lett. **89**, 011301 (2002).
[22] H. S. Lee, K. T. Matchev, and T. T. Wang, Phys. Rev. D **77**, 015016 (2008); H. S. Lee, C. Luhn, and K. T. Matchev, arXiv:0712.3505; H. S. Lee, Phys. Lett. B **663**, 255 (2008).
[23] R. Barbier *et al.*, Phys. Rep. **420**, 1 (2005).
[24] H. Dreiner and G. Ross, Nucl. Phys. **B365**, 597 (1991).
[25] B. Allanach *et al.* (R parity Working Group Collaboration), arXiv:hep-ph/9906224.
[26] B. C. Allanach, M. A. Bernhardt, H. K. Dreiner, C. H. Kom, and P. Richardson, Phys. Rev. D **75**, 035002 (2007).
[27] S. Dimopoulos and L. Hall, Phys. Lett. B **207**, 210 (1988).
[28] S. Dimopoulos, R. Esmailzadeh, L. J. Hall, and G. D. Starkman, Phys. Rev. D **41**, 2099 (1990).

[29] H. Dreiner, P. Richardson, and M. H. Seymour, Phys. Rev. D **63**, 055008 (2001); arXiv:hep-ph/9903419; arXiv:hep-ph/0001224.

[30] G. Moreau, E. Perez, and G. Polesello, Nucl. Phys. **B604**, 3 (2001).

[31] F. Deliot, G. Moreau, and C. Royon, Eur. Phys. J. C **19**, 155 (2001).

[32] B. C. Allanach, M. Guchait, and K. Sridhar, Phys. Lett. B **586**, 373 (2004).

[33] V. M. Abazov *et al.* (D0 Collaboration), Phys. Rev. Lett. **89**, 261801 (2002).

[34] V. M. Abazov *et al.* (D0 Collaboration), Phys. Rev. Lett. **97**, 111801 (2006).

[35] D. Choudhury, S. Majhi, and V. Ravindran, Nucl. Phys. **B660**, 343 (2003).

[36] L. L. Yang, C. S. Li, J. J. Liu, and Q. Li, Phys. Rev. D **72**, 074026 (2005).

[37] H. K. Dreiner, S. Grab, M. Kramer, and M. K. Trenkel, Phys. Rev. D **75**, 035003 (2007).

[38] Y. Q. Chen, T. Han, and Z. G. Si, J. High Energy Phys. 05 (2007) 068.

[39] F. Borzumati, J. L. Kneur, and N. Polonsky, Phys. Rev. D **60**, 115011 (1999).

[40] G. Moreau, M. Chemtob, F. Deliot, C. Royon, and E. Perez, Phys. Lett. B **475**, 184 (2000).

[41] M. Chaichian, A. Datta, K. Huitu, S. Roy, and Z. h. Yu, Phys. Lett. B **594**, 355 (2004).

[42] B. C. Allanach, H. K. Dreiner, P. Morawitz, and M. D. Williams, Phys. Lett. B **420**, 307 (1998).

[43] M. Chemtob, Prog. Part. Nucl. Phys. **54**, 71 (2005).

[44] H. K. Dreiner, M. Kramer, and B. O'Leary, Phys. Rev. D **75**, 114016 (2007).

[45] B. C. Allanach, A. Dedes, and H. K. Dreiner, Phys. Rev. D **60**, 075014 (1999).

[46] K. Agashe and M. Graesser, Phys. Rev. D **54**, 4445 (1996).

[47] B. C. Allanach, A. Dedes, and H. K. Dreiner, Phys. Rev. D **60**, 056002 (1999).

[48] Even if one assumes that the one-loop contributions to the neutrino mass are suppressed, two-loop contributions lead to a bound on λ'_{333} of 10^{-2} [49,65], which still leads to a suppressed cross section.

[49] F. Borzumati and J. S. Lee, Phys. Rev. D **66**, 115012 (2002).

[50] A. Belyaev, M. H. Genest, C. Leroy, and R. R. Mehdiyev, J. High Energy Phys. 09 (2004) 012.

[51] G. Corcella *et al.*, J. High Energy Phys. 01 (2001) 010.

[52] G. Corcella *et al.*, arXiv:hep-ph/0210213.

[53] H. K. Dreiner, P. Richardson, and M. H. Seymour, J. High Energy Phys. 04 (2000) 008.

[54] B. L. Combridge, Nucl. Phys. **B151**, 429 (1979).

[55] H. Dreiner and R. Phillips, Nucl. Phys. **B367**, 591 (1991).

[56] A. Datta, J. M. Yang, B. L. Young, and X. Zhang, Phys. Rev. D **56**, 3107 (1997); T. Han and M. B. Magro, Phys. Lett. B **476**, 79 (2000); A. Belyaev, M. H. Genest, C. Leroy, and R. R. Mehdiyev, J. High Energy Phys. 09 (2004) 012.

[57] J. Pumplin, A. Belyaev, J. Huston, D. Stump, and W. Tung, J. High Energy Phys. 02 (2006) 032.

[58] For simplicity, we do not include the supersymmetric QCD corrections given in [37], since we must then include a discussion of the dependence on the soft supersymmetry breaking parameters. It was shown in [37] that supersymmetric QCD corrections can change the total hadronic cross section by more than $\pm 20\%$.

[59] R. Bonciani, S. Catani, M. L. Mangano, and P. Nason, Nucl. Phys. **B529**, 424 (1998).

[60] M. Cacciari, S. Frixione, M. L. Mangano, P. Nason, and G. Ridolfi, J. High Energy Phys. 04 (2004) 068.

[61] S. h. Zhu, Phys. Rev. D **67**, 075006 (2003).

[62] T. Plehn, Phys. Rev. D **67**, 014018 (2003).

[63] H. L. Lai *et al.*, Phys. Rev. D **55**, 1280 (1997).

[64] We thank Jean-Loic Kneur for private discussions on the parameters used in Ref. [39].

[65] E. Accomando *et al.*, arXiv:hep-ph/0608079.

[66] S. Dawson, Nucl. Phys. **B261**, 297 (1985).

[67] H. K. Dreiner, S. Heinemeyer, O. Kittel, U. Langenfeld, A. M. Weber, and G. Weiglein, arXiv:0707.1425; H. K. Dreiner, C. Hanhart, U. Langenfeld, and D. R. Phillips, Phys. Rev. D **68**, 055004 (2003); D. Choudhury, H. K. Dreiner, P. Richardson, and S. Sarkar, Phys. Rev. D **61**, 095009 (2000).

[68] B. C. Allanach, M. A. Bernhardt, H. K. Dreiner, S. Grab, C. H. Kom, and P. Richardson, arXiv:0710.2034.

[69] S. Dittmaier, P. Uwer, and S. Weinzierl, Phys. Rev. Lett. **98**, 262002 (2007).

[70] J. A. Aguilar-Saavedra *et al.*, Eur. Phys. J. C **46**, 43 (2006).

[71] E. Boos *et al.*, arXiv:hep-ph/0109068.

[72] The version of HERWIG used in this paper includes modifications to simulate the four-body decays of the stau LSP and is available on request from Peter Richardson.

[73] K. Odagiri, J. High Energy Phys. 10 (1998) 006.

[74] B. C. Allanach, Comput. Phys. Commun. **143**, 305 (2002); B. C. Allanach and M. A. Bernhardt, Report No. BONN-TH-2007-06.

[75] S. Frixione and B. R. Webber, arXiv:hep-ph/0612272.

[76] S. Frixione, P. Nason, and B. R. Webber, J. High Energy Phys. 08 (2003) 007.

[77] F. Maltoni and T. Stelzer, J. High Energy Phys. 02 (2003) 027.

[78] CMS Collaboration, CERN Report No. CERN-LHCC-2006-021, 2006.

[79] The PXCONE algorithm by L. Del Pozo and M. H. Seymour is publicly available as part of the FASTJET package from http://www.lpthe.jussieu.fr/~salam/fastjet/.

[80] M. T. Bowen, Phys. Rev. D **73**, 097501 (2006).

[81] J. H. Kuhn and G. Rodrigo, Phys. Rev. D **59**, 054017 (1999).

[82] L. G. Almeida, G. Sterman, and W. Vogelsang, arXiv:0805.1885.

[83] B. C. Allanach *et al.*, Eur. Phys. J. C **25**, 113 (2002).

[84] S. Blusk, O. Buchmuller, A. Jacholkowski, T. Ruf, J. Schieck, and S. Viret, Report No CERN-2007-004.

[85] H. P. Nilles, Phys. Rep. **110**, 1 (1984).

[86] H. E. Haber and G. L. Kane, Phys. Rep. **117**, 75 (1985).

[87] S. P. Martin, arXiv:hep-ph/9709356.

[88] I. J. R. Aitchison, arXiv:hep-ph/0505105.